Journal of the Meteorological Society of Japan

EARLY ONLINE RELEASE

The DOI for this manuscript is

DOI:10.2151/jmsj.2022-047

J-STAGE Advance published date: August 25th, 2022

The final manuscript after publication will replace the preliminary version at the above DOI once it is available.

Development of a nocturnal temperature inversion in a small basin associated with leaf area ratio changes on the mountain slopes in central Japan

Kenji KUSUNOKI

Nomura Research Institute, Ltd.
Tokyo, Japan

and

Kenichi UENO[1]

Faculty of Life and Environmental Sciences
University of Tsukuba, Tsukuba, Japan

August 3, 2022

----

1) Corresponding author: Kenichi UENO,
Faculty of Life and Environmental Sciences, University of Tsukuba, Teno-dai 1-1-1, Tsukuba, Ibaraki 305-8572 JAPAN
Email: ueno.kenichi.fw@u.tsukuba.ac.jp
Tel/fax: +81-298-53-4399

Abstract

Nocturnal temperature inversion (NTI) is an important factor characterizing the local climate in mountainous areas. In central Japan, most of the mountain slopes are covered by forests, but the effects of their leaf expansion/fall on the NTI variations in basins have not been clarified. According to a three-year leaf area index (LAI) observation in the mixed forest of the Sugadaira Highland (1320 m a.s.l.), Nagano Prefecture, Japan, we identified weakening of the NTI associated with leaf expansion and strengthening after leaf fall in a small basin. Using digital elevation and land-cover data, we defined the distribution of the deciduous and mixed forests in the catchment area of nocturnal cold air drainage. The estimated timings of leaf expansion/fall at the catchment scale based on the effective cumulative temperature almost coincided with the NTI changes. Micrometeorology observations showed that NTI at the forest floor and downslope winds at the adjacent grassland strengthened during the dormant (leafless) season in the nighttime when the radiative cooling is strong. Calm and clear nights were chosen during the spring dormant season and the summer growing season for 22 and 30 nights, respectively. The heat loss during the cold-air pool development was estimated, and converted to storage heat flux in the forest areas. The storage heat flux was 3.8 W/m² more on average in the growing season than the dormant season, and it was less than that of forests estimated in previous studies (several 10 W/m²), indicating that an increase in storage heat flux of the forests

with leaf expansion could cancel nocturnal radiative cooling and weaken gravity currents at the forest floor.

Keywords: leaf area index, mountain forest, temperature inversion, cold-air pool

1. Introduction

Forests are acting as an interface in exchanging water-energy flux between land surface and the atmosphere (Mencuccini et al. 2003). At mesoscale, they control the heat budget through the change in albedo, interception and evapotranspiration at the crown and indirectly modify the process of cloud formation and water cycle (Ellison et al. 2017; Bosman et al. 2018). At microscale, they increase the roughness in the atmospheric boundary layer absorbing the momentum flux and reduce the surface wind speed (Garratt 1992). Forest crowns shield the forest floor from sunshine and increase downward long-wave radiation, which reduces diurnal change in the surface air temperature (Hardwick et al. 2015; Geiger et al. 2003). Such mitigation effects could change not only the ecosystem environment in the forests (Arx et al. 2013; De Frenne et al. 2013) but also the microclimate around the forests including soil erosion processes at the floor (Ueno et al. 2015).

People in montane areas tend to live in the basin and valley where nocturnal temperature inversion (NTI) prevails, and the evolution of the cold-air pool with the NTI is sensitive primarily to ambient atmospheric conditions (Dorninger et al. 2011). On the other hand, Kiefer and Zhong (2013) demonstrated by a numerical study that sidewall forests strongly affect the temperature inversion to develop cold-air pools. In Japan, the atmospheric heat budget in a basin and thermally induced local circulations between the central mountain areas and the Kanto Plain have been investigated (e.g., Kondo et al. 1989; Kimura and Kuwagata 1993; Lee and Kimura 2001). Enhancement of the coastal precipitation system or local circulation in the basin due to mountain-induced katabatic winds has been reported (Tachibana 1995; Uehara et al. 2020). Iijima and Shinoda (2000) identified the seasonal differences of the cold-air pool formation in a hollow in the subalpine areas of the Yatsugatake Range. However, those studies did not consider mountain forests explicitly as a surface boundary condition, and their contribution to the nocturnal local climate has not been fully discussed.

The effects of global-scale climate change on the phenology of mountain forests have been indicated (Diaz et al. 2003). For instance, a longer growing season for deciduous forests due to global warming has been reported (Menzel et al. 2006; Vitasse et al. 2009). Changing of the forest phenology could modify the air temperature and precipitation pattern in the surrounding environments through mesoscale boundary-layer dynamics (Hogg et al. 2000). Wind and stability below the canopy in a deciduous forest causes evident contrasts between the leaf-on and -off seasons against the mountain-valley circulations (Wang et al. 2015). Devito and Miller (1983） observed that nocturnal cold air drainage prevailed in the forest during the leafless phase, and Staebler and Fitzjarrald (2005) noted that the impact of leaf area changes on sub-canopy flows is more evident at night. Froelich et al. (2011) pointed out the importance of considering the heat storage of physical elements in the canopy to model canopy air cooling. Swenson et al. (2019) also demonstrated that biases in the surface heat flux estimated by the community land model relates to the lack of heat storage in vegetation biomass.

In central Japan, many of the cool temperate forests in mountainous areas are composed of deciduous trees, such as the Japanese larch. Tadaki et al. (1994) studied the altitudinal dependency of the growth of deciduous tree leaves on temperature, and Nagai et al. (2015) detected the timing of leaf expansion/fall at different altitudes using satellite data, and evaluated the relationship between the timing and daily mean temperature using Automated Meteorological Data Acquisition System (AMeDAS) data from the Japan Meteorological Agency (JMA). Most of the AMeDAS stations are located in the valley or basin in mountainous areas, and a small number of them were more than 1000 m above sea level (a.s.l.). Therefore, applying extrapolation for temperature estimation at high elevations is done without consideration of the effects of forest phenology in the neighboring mountains on the AMeDAS data.

Local climate changes in the Sugadaira Highland, Nagano Prefecture, Japan, have been observed using multiple automatic weather stations with a forest tower placed in the mixed forest of Sugadaira Research Station (SRS), part of the Mountain Science Center of the University of Tsukuba. This study revealed relations between the seasonal change in leaf area index (LAI) and the formation of a cold-air pool over a small basin during snow-free seasons. Specifically, the microscale meteorology around the forest was observed to identify the formation of nocturnal gravitationally induced drainage flows as a function of LAI changes during the highland-scale radiative cooling nights. We also assessed catchment-area LAI changes that could contribute to the storage heat flux of daytime forest and compared them with the amounts of heat loss to develop cold-air pool estimated for each before and after the leaf expansion.

2. Data and Method

2.1 Study area

The Sugadaira Highland area is 36.51–36.55ºN, 138.30–138.36ºE (Fig. 1a), with an altitude range of 1200–1500 m a.s.l., along the western slope of Mt. Nekodake (2207 m) (Fig. 1b). The highland is located between the Nagano (at northwest) and Ueda (at southwest) basins, where the synoptic winds prevail along a south–north direction around the western edge of the Echigo mountain range. A small basin (called the Sugadaira basin) exists between Mt. Ohmatsuyama (1649 m) and Mt. Taroyama in the highland. Croplands and sports grounds occupy in the basin bottom, and the mountain slopes are covered by deciduous trees (mostly *Larix kaempferi* (Japanese larch), *Betula platyphylla* (Japanese white birch), and *Quercus crispula* (Japanese oak)) and evergreen trees (mostly *Pinus densiflora* (Japanese red pine)). Grasslands used for gelande and pastureland also spread along the mountain slopes where Nakamura (1976, 1978) observed the characteristics of gravity currents due to radiative cooling. Kudoh et al. (1982) and Toritani (1985) revealed the development of an inversion layer with an 80–90 m depth in the basin synchronizing the occurrence of gravity currents in the case of calm nocturnal weather.

The land-cover condition of the highland was captured in the 2015 European Space Agency Climate Change Initiative Land Cover (ESA CCI-LC) data (Defourny et al. 2017). Synoptic-scale weather conditions, especially for the identification of calm and clear nights, were diagnosed using fifth-generation European Centre for Medium-Range Weather Forecasts (ECMWF) atmospheric reanalysis (ERA5) data (Hersbach et al. 2020) and JMA Meso-Scale Model (MSM) data. The grid and temporal scales of each objective analysis data set are 0.1*0.125 degrees resolution and every 3 hours for constant pressure levels and 0.05*0.0625 degrees and every hour at the surface, respectively. Digital Elevation Model (DEM) data with a 5 m interval, produced by the Geospatial Information Authority of Japan, was used to determine a catchment producing nocturnal cold air drainage to contribute cold-air pool formation. Snow-cover fractions were identified by the 500 m interval snow ratio data provided by the Moderate Resolution Image Spectroradiometer, NASA and Visible Infrared Imaging Radiometer Suite, Snow and Ice Global Mapping Project (MOD10A1 Snow Products, Hall and Riggs 2016).

2.2 Observation sites

Fixed-point meteorological observation was conducted at the Sugadaira AMeDAS station

(AME, 36.533°N, 138.325°E, 1253 m a.s.l.) and SRS1 at the SRS (36.524°N, 138.347°E, 1320 m a.s.l.), where the air temperature (1.5 m level, platinum resistance thermometer with a ventilated shield, 0.1 ℃ accuracy), precipitation (0.5 mm heated tipping bucket with a wind shield), and snow depth (laser sensor, 1 mm accuracy) were measured (Fig. 1b,c). The temperature difference between the AME and SRS1 was used to detect the NTI over the Sugadaira basin.

The SRS area is composed of grasslands (6 ha) and forests (22.5 ha) covered with *Sasa albo-marginata* at the floor (Fig. 1c). The forests are composed of evergreen trees (4 ha), predominantly Japanese red pine, and deciduous broadleaf trees (14 ha). Mixed forests (4.5 ha) are distributed in the center (marked with an X in Fig. 1c), where a temperature profile at 6 levels with solar radiation, wind direction/speed, and atmospheric pressure at the tower top (about 22 m high) were observed by an automated weather station (RX3000 data logger with smart sensors, Onset Co.) as the forest tower station (FTS, 36.521°N, 138.353°E, 1335 m). Using this station, Ueno et al. (2017) reported that the shading effects of tree crowns under different forest phenology conditions affected the diurnal and seasonal variation of temperature gradients in the forest. An LAI sensor (MIJ-15LAI, Environmental Measurement Japan Co.) was set near the forest tower (4 m south, 2 m above the ground) on April 2018, where seasonal changes in photosynthetically active radiation (PAR, 400–700 nm) and near-infrared radiation (NIR, 700–1000 nm) were automatically measured.

Meteorological conditions outside the forest, such as wind speed and direction at 3 m, temperature and humidity at 1.3 m and 3 m above ground level, were monitored at the campus grass site (CGS) using the same type of an automated weather station at the FTS. A four-component (upward/downward short/long-wave) radiation sensor (CNR4, Kipp&Zonen Co.) was also set, and net radiation (Rn) was measured. Thermistor temperature sensor with a data logging system (U23 and THB type, Onset Co.) at the FTS and CGS were equipped with a natural ventilated shield (0.2 ℃ accuracy and 3-minute time constants in catalog specification). Additional air-temperature observations were conducted using the U23 type system at 3 m with a standing pole from August 2020 to July 2021 at three points (1258 m, 1295 m, and 1456 m, indicated by crosses in Fig. 1b) to monitor the depth of the NTI (observation at 1456 m terminated on November 2020). The data interval was 10 minutes except for 1 hour at the AME and SRS1. In winter, a snow depth of around 80 cm occurs in the SRS with heterogeneous redistribution due to windy weather (Ueno et al. 2007). The snow-cover condition was monitored using snow-depth sensors at AME and SRS1 and an albedo sensor at the FTS to identify snow-covered periods.

3. Results

3.1 Seasonal change in the LAI and nocturnal inversion layer

Using LAI sensor data, the LAI was measured and estimated every 10 minutes using an empirical formula from Kume et al. (2011) based on the tendency of more absorption/scattering of PAR than NIR at the forest floor due to an increase in the LAI at the crown. As the sensors measure instantaneous radiation without a ventilation system, estimated values sometimes showed an abnormal range with snow/leaf caps, direct insolation, and sunfleck. This study filtered original 10-minute interval data to obtain daily values according to the following steps: (1) daytime values during 10:00–14:00 Japan Standard Time (JST) were used; (2) only the cloudy periods (solar radiation in a 50–500 W/m² range at the top of the tower) were nominated; (3) data with $(NIR - PAR)/PAR$ between 0.2 and 1.5 were used; (4) LAI values more than $\pm\sigma$ (standard deviation) from the daily average were excluded, and the candidates were re-averaged to obtain daily data.

Intraseasonal changes of the daily LAI at the FTS were examined for three years (2018–2020) (Fig. 2a). The records showed an increase in LAI around 3 m²/m² from May to September and a decrease to around 1 m²/m² from October to April (Fig. 2a), obviously indicating the leaf expansion and leaf fall from those deciduous trees. The Increase rate of the LAI in spring was larger than the rate of decrease in autumn, especially in 2018. Nasahara et al. (2008) observed a seasonal change in canopy LAI from 0 to 5 m^2m^{-2} using LAI-2000 and TRAC sensors based on indirect optical methods at the Takayama site in Gifu Prefecture, central Japan. Kuribayashi et al. (2020) measured the LAI change at the SRS for larch trees using the interval camera method, showing similar timing of leaf expansion and leaf fall with a slightly different amplitude. We defined the dormant season (spring/autumn), leaf-expansion season, growing season, and leaf-fall season using thresholds of 1.5 and 2.0 m^2m^{-2} of the daily LAI for three years (Table 1a).

Seasonal changes in the daily maximum snow depth at the AME and SRS1 sites (Fig.2b) were compared with daily albedo changes at the FTS (Fig. 2c), where the daily albedo is calculated by averaging daytime (10:00–14:00 JST) 10-minute interval values and screening out the abruptly low values due to snow caps and precipitation. There are 67 m altitudinal differences between the AME and SRS1, but the tendency of day-to-day snow-depth change was similar. Snow-cover periods (more than 30 days of continuous snow) at SRS1 occurred from December to April, as summarized in Table 1b. The albedo changed at the FTS indicated that snow cover also existed in the forest for periods similar to those at SRS1 except for the later increase in albedo around 350-365 DOY (day of year) due to *Sasa albo-marginata* at the forest floor that interrupted the ground snow cover. Comparing Table 1a and b, it is clear that the timing of the leaf expansion/fall in the mixed forest and the start/end of snow cover is different among years. The winter of 2019–2020 was extremely warm with a short snow-cover period; however, the timing of leaf expansion in 2020 was not different from that in other years. We speculated that the effective cumulative temperature (ECT) of the precursor months (such as April and May) in 2020, which could affect the leaf expansion of deciduous trees, was not much different from those in other years.

Temporal changes in the surface air-temperature difference between the AME and SRS1 for eight years, as functions of DOY and JST, are shown in Fig. 3. The blue (negative) areas indicated the occurrence of NTI (the temperature at the AME is cooler than that at SRS1). The NTIs were dominant in cold seasons and they were sometimes interrupted due to windy days by synoptic-scale disturbances (figures omitted). Furthermore, the NTI was diminished in the warm season, such as DOY 150–270. The start/end of the snow-cover and leaf-expansion/fall seasons at the FTS, summarized in Table 1, are indicated by blue arrows and red bars after 2017 winter Fig. 3. It is surprising that the timing of leaf expansion/fall clearly corresponded to that of the weakening/strengthening of the NTI, whereas the starts/ends of snow cover were not related. Additional air temperature observations between the AME and SRS1 (at cross marks in Fig. 1b) showed that the NTI was mostly limited below the altitude of the SRS, and the thickness of the NTI increased as the temperature difference between the AME and SRS1 increased. In other words, the negative temperature difference in Fig. 3 indicates the development of a nocturnal cold-air pool in the Sugadaira basin. Namely, evolution of the nocturnal cold-air pool corresponded to the seasonal LAI changes of the forest crown in the upstream mountain slope.

3.2 Behavior of nocturnal downslope winds around the forest

Drainage flows on the mountain slopes start with the onset of radiative cooling to develop a nocturnal cold-air pool in the basin (Mahrt and Heald 2015). Maki et al. (1986) demonstrated that about 80% of the observed cooling of the whole nocturnal boundary layer in a basin is attributed to horizontal advective cooling from the surrounding mountain slopes when the winds of free atmosphere are weak. We examined the seasonal changes in surface winds around the forest in relation to the development of the cold-air pool. First, calm and clear nights, which are conducive to the forming of a cold-air pool, were selected using MSM and AME data following criteria such as (A) no daily precipitation records at the AME with (B) an averaged (maximum) wind speed from the MSM data at 850 hPa from 18:00 JST to 6:00 JST of less than 7 m/s (9 m/s) at the closest grid point (36.5°N, 138.375°E). The thresholds of wind speed were determined based on the results of Petkovsek (1992). The days with snow cover observed at the AME and MOD10A1 snow products in the Sugadaira Highland were excluded. Seasonal changes in the nocturnal (from sunset to sunrise) averaged surface air-temperature gradient (SATG) and wind speed in the downslope direction (WSDD) at the CGS outside the mixed forest were compared with the changes in LAI and intensity of the temperature inversions (ITIs) at the FTS in the forest in 2019 as shown in Fig. 4. The SATG is a vertical temperature gradient calculated as the 1.3 m temperature minus 3.0 m one at the CGS and the 1.0 m one minus the 5.3 m one at the FTS with normalized by the distance. The ITI is the integration of the hourly temperature difference between the AME (1253 m) and SRS1 (1320 m) when the AME temperature is lower than that of SRS1 during the hours from sunset to sunrise. The negative SATGs, indicating a stable surface boundary layer at night, dominated at CGS (grassland) throughout the season as shown by black dots in Fig. 4b. Weak inversion also occurred at FTS (in the forest) in the dormant seasons as shown by white dots, but it almost disappeared during the growing season. The disappearance of temperature gradient at the forest floor may be corresponded with the reduction in radiative cooling due to the increase in downward long-wave radiation as observed by Ueno et al. (2017). Additionally, the WSDD at the CGS clearly diminished during the growing season (Fig. 4c) with the reduction of the ITI (Fig. 4d). We could not observe the WSDD in the forest with the automatic weather station because the wind speed was mostly weaker than the detectable range of mechanical wind speed sensor; however, temporal surface wind speed observation using an ultrasonic anemometer from August to November 2020 at the FTS showed an increase in WSDD with the LAI decrease (figures omitted). The results indicated that nocturnal downslope winds were reduced both at the grassland surface and at the forest floor with the weakening of cold-air pool development, even though the stable surface boundary layer prevailed outside the forest.

Seasonal differences in the long-wave radiation balance primarily change the intensity of nocturnal cooling in a high mountain hollow (Iijima and Shinoda, 2002). Maki and Harimaya (1988) revealed that reduction of downward long-wave radiation affected by the accumulation of cold air in the basin is fed back to enhance the nocturnal cooling at the basin bottom, especially in a deep basin such as at a depth (surrounding mountain height) of 500 m. However, this effect was small for the shallow basin less than 100 m depth such as the Sugadaira basin. Again, we compared the SATG and WSDD/ITI between the high and low LAI days (corresponding to growing and dormant seasons) in Fig. 5 as a function of surface Rn for three years on clear and calm nights without snow cover, where the surface Rn was adopted from the nearest grid point value on the ERA5 data (Rn-ERA) to represent a mesoscale radiative cooling condition over the highland. The Rn-ERA showed significant correlation with the Rn observed at the CGS, and seasonal changes in Rn at the CGS did not relate to forest growth/leaf fall (figures omitted). Therefore, the variance of Rn-ERA in Fig.5 is mainly dependent on the seasonal change in mesoscale surface skin temperature, including the effects of downward long-wave radiation from the atmosphere, as demonstrated by Maki and Harimaya (1988), and cloud covers. A nocturnal negative SATG (i.e., stable surface boundary layer) prevailed in the grassland for high and low LAI days and strengthened on stronger radiative cooling nights (less than around -60 W/m^2 in the Rn-ERA) (Fig. 5a). In the forest, the tendency for SATG is the same for high LAI days but was depressed for low LAI days (Fig. 5b). In the grassland, the WSDD increased (down-slope winds prevailed) on stronger radiative cooling nights only for low LAI days (Fig. 5c). Differences between the growing and dormant seasons were evident especially for stronger radiative cooling nights, and they were associated with increases in the ITIs (Fig. 5d-right). The tendency confirmed that nocturnal downslope winds contributing to the development of the cold-air pool were especially enhanced during the dormant season with the highland-scale strong radiative cooling condition.

3.3 Heat-budget assessment

Heat-budget analysis has been proposed as a basic methodology to assess the consistency of nocturnal boundary-layer development and radiation balance (e.g., Kondo et al. 1989). The consistency of cold-air pool development due to a decrease in the LAI was examined by means of a simple heat-budget theory, paying special attention to canopy heat storage. A basic land-surface heat budget without advection terms can be described by the following formula (1) during a snow-free season:

$$R_n = H + E + G \qquad (1),$$

where *Rn*, *H*, *E*, and *G* represent net radiation, sensible heat, latent heat, and ground heat flux, respectively. If we consider the heat flux at the forest canopy level, the formula can be modified as follows:

$$R_n = H + E + S \qquad (2),$$

where *S* represents the storage heat flux by the forest (Bernhofer et al. 2003). Similar to *G*, *S* can be ignored when we discuss the daily mean base heat budget. However, many previous studies have revealed that forests absorb large amounts of S during the day and release it at night. For example, Oliphant et al. (2004) estimated *S* to have an amplitude of 60 W/m^2 with a high LAI during the growing season, furthermore, they indicated that the percentage of foliage heat storage in *S* is small. In Japan, Saitoh et al. (2010) estimated more than 40 W/m^2 of *S* at the Takayama observation site with various biotic activities, such as

$$S = S_H + S_E + S_V + S_C \qquad (3),$$

where S_H and S_E are the sensible and latent heating in the forest, respectively; S_V is the storage term by the forest body; and S_C is the amount of photosynthesis and respiration.

During the growing season, S_E and S_C increase, and S_C reaches 12 W/m² during the day and 7 W/m² at night (Saitoh et al. 2010). The heat budget, including *S*, and net radiation over and beneath the deciduous forest canopy abruptly change depending on the leaf emergence and senescence (Wilson et al. 2000; Wilson and Baldocchi 2000). As shown in Fig. 5, a lower LAI condition enhanced the SATG and ITI even under the similar mesoscale strong radiative cooling condition. We hypothesized that nocturnal radiative cooling from the crown was offset by the accumulated daytime S during the growing season, and it weakened the katabatic drainage flow from the mountain slope to develop the cold-air pool. In Fig. 3, the end of NTI (right sides of blue colored area) occurred almost at the same time as the sunrise. However, the start of the NTI was rather variable depending on the day, implying that the day-to-day variability of daytime *S* with various insolation conditions contributed to the speed to develop a cold-air pool after sunset.

Previous sections used an LAI point measured at the FTS to discuss the linkage between the variability in nocturnal downslope winds and the temperature inversion layer. The actual *S* depends on the tree species and their ages and numbers, and areal evaluation of *S* in the mixed forests or even at the catchment scale is difficult using point measurements. Timing of leaf expansion/leaf fall also shifts depending on the elevation and local topography (e.g. Pellerin et al. 2012). Therefore, this study estimated the heat-amount difference in the atmospheric volume over the basin with and without apparent NTI, corresponding to the dormant and growing seasons, and compared it with the *S* estimated in previous studies.

The following steps were conducted; (ⅰ) defining a catchment of the basin (drainage area) in the Sugadaira Highland that provides gravity currents, (ⅱ) comparing LAI changes measured a point and at the catchment-scale to consider the timing shift of leaf expansion/leaf fall, and (ⅲ) calculating the amounts of atmospheric heat loss to form the cold-air pool.

For the step ⅰ, nocturnal gravity currents in the surface boundary layer were assumed to run off as land-surface water flow. At first, a 5 m interval DEM was smoothed in a spatially moving average within 3*3 grids to filter the microtopography. An area of a basin bottom (surrounded by a solid line in Fig. 6a) was set, and adjacent grids with higher elevation were included as a target catchment on the 30 m interval. This interval was adjusted to the grid size of the ESA CCI-LC data. Figure 6a shows the drainage area with four land-cover types defined in the ESA CCI-LC data, where pastures (including grassland, cropland, and sports grounds), mixed forests, and deciduous forests occupy 48 %, 17 %, and 32 % of the area, respectively. The mixed forest of the FTS in the SRS exists at the southern edge of the basin (marked by an X in Fig.6a), but it was categorized as a deciduous forest by the ESA CCI-LC data. Figure 6b shows the altitudinal changes in the occupancy of land covers. The forest percentage increases above the 1400 m level, compared to the percentage of grassland/cropland, except at the 1600 m level, at which deciduous-tree and mixed forests occupy 65 % of the total coverage of the forests.

Nagai et al.（2015）investigated the timing of the start/end of the growing season for deciduous trees in central Japan, which can be estimated based on the ECT (effective cumulative temperature) using daily AME temperature data (Ti) with following formulas:

$$ECT_{SGS} = \sum_{i=D_{s\_spring}}^{D_{SGS}} \max(T_i - T_{ct\_spring}, 0) \quad (4)$$

$$ECT_{EGS} = \sum_{i=D_{s\_autumn}}^{D_{EGS}} \min(T_i - T_{ct\_autumn}, 0) \quad (5),$$

where i is the date, ECT_{SGS} and ECT_{EGS} are the required ECT to start and end the growing season, respectively; D_{SGS} and D_{EGS} are the starting and ending dates of the growing season, respectively; and D_{s_spring} and D_{s_autumn} are the starting dates of the calculation for spring and autumn, January 1 and September 1, respectively. According to the definition by Motohka et al. (2010), the growing season for which to apply those formulas includes the leaf-expansion and leaf-fall season in this study (e.g., Table 1a). Formula (4) is used for spring and (5) for autumn. T_{ct} is a threshold temperature set as 2 ℃ for (4) and 18 ℃ for (5) in central Japan. For step ii , ECT_{SGS} and ECT_{EGS} were first estimated based on the starting date of the leaf-expansion season and the ending date of the leaf-fall season, respectively, using the LAI observation at the FTS. This study assumed that mixed and deciduous forests in the drainage area expand/drop leaves with the same ECTs observed at the FTS. Then, the ECT at each altitude was accumulated, and the starting date of the leaf-expansion season and ending date of the leaf-fall season were defined as when they reached the ECT_{SGS} and ECT_{EGS} of the FTS, respectively. The T_i at each altitude was interpolated using the lapse rate between the AME and SRS1 below 1320 m a.s.l. Above the SRS1, the temperature was extrapolated using 0.6 ℃/100 m based on the previous observation of

Ueno et al. (2013).

The calculation was conducted for 2018–2020, and the DOYs of the start of the leaf-expansion season and the end of the leaf-fall season were averaged to show the catchment-scale duration of the growing season with altitudinal transition as shown in Fig. 7a. Seasonal changes in the observed daily LAI at the FTS (1335 m) are also shown in Fig. 7b. According to our estimation, it takes almost one month to complete the leaf-expansion and leaf-fall season within the drainage area. If we focus on the mountain side slopes around the basin below 1600 m, leaf-expansion/fall was almost completed within two weeks. Even if we considered those catchment-scale time lags of the leaf expansion/fall (such as around DOY 10–20) as part of the time range on the red bars in Fig. 3, the timings of abrupt change in NTI were almost the same as the basin-scale LAI changes.

Regarding step iii, clear and calm nights without snow cover from April 2013 to September 2020 were nominated to increase number of samples for heat budget analysis. Catchment-scale dormant/growing seasons were redefined in each year using the three years average of ECT_{SGS} and ECT_{EGS} at FTS, where “catchment scale” of each season is defined as the periods when all of the elevations were categorized as being in a non-growing (dormant) or growing season. Candidates were 112 days in the dormant season (spring), 378 days during the growing season, and 48 days in the dormant season (autumn). As the depth of the temperature inversion cannot be identified in this study, the amount of heat loss in the air according to the NTI development was calculated from below 1320 m to the basin bottom beginning at sunset for 6 hours. Based on the past observational study by Toritani (1985), the upper elevation as 1320 m is reasonable to capture the NTI. We confirmed that temperature at the AME and the southeastern point at the basin bottom correlated with each other, indicating that the AME temperature is representative of the basin bottom. To highlight the condition of nocturnal radiative cooling, night-averaged Rn values at the nearest grid point of the ERA5 data within -70 to -60 W/m² were extracted for 23 nights in the spring dormant season and 31 nights in the growing season. For the candidate days, the hourly potential temperature was calculated at 10 m altitude intervals by temperature interpolation between the AME and SRS1 and atmospheric pressure at SRS1.

The amounts of heat loss (ΔL_j) required for temperature cooling at certain altitude (j) was calculated as follows;

$$\Delta L_j = C_p M_j \Delta\theta_j \qquad (6),$$

$$M_j = \rho_j A_j d \qquad (7),$$

where C_p is the specific heat of constant pressure, Mj is the mass of air, $\Delta\theta_j$ is an estimate of the decrease in potential temperature from sunset to 6 hours later at a certain elevation, ρ_j is the density estimated based on the pressure and temperature at the AME, A_j is the area, and d is a layer thickness as 10 m. Then ΔL_j was accumulated from the basin bottom (1230 m) to SRS1 (1320 m) to derive the total amounts of heat loss in the air (L) to develop the cold-air pool. The average of L became $2.42*10^6$ MJ and $1.29*10^6$ MJ before and after a transition season of leaf expansion, respectively, and the difference was $1.13*10^6$ MJ.

When the cooling is attributed to the heat-budget difference in the deciduous and mixed forest areas (13.75 km²), the difference corresponds to 3.80 W/m² in averaged storage heat flux per unit area above the forest (*Ldif*). Previous studies (e.g., Oliphant et al. 2004; Moderow et al. 2009; Saito et al. 2010) indicated the order of *S* as several 10 W/m², and the estimated *Ldif* became smaller. As the basin topography opens in the southeast direction, cold air may leak into the downstream, and the *Ldif* would be underestimated. However, the *Ldif* cannot exceed the *S* of previous studies. Namely, the heat-amount difference in cold-air pool development according to cold-air advection and accumulation was nearly the same or smaller order than the total storage heat flux of forest estimated by the previous studies.

4. Summary and discussion

This study found abrupt changes in the development of the nocturnal cold-air pool in a small basin associated with leaf expansion and leaf fall at a mountain slope mixed-forest site for multiple years. A catchment-scale estimation for the timing of leaf expansion/fall using the ECT coincided with the NTI changes. Croplands in the pasture (Fig. 6), where lettuce is cultivated, occupy 15 % of the land, and they change the seasonal landcover condition. However, the occupancy area is small, and the timing of planting/mowing differs from the LAI changes (Fig.3) and the snow-cover condition. Therefore, the NTI changes were not due to the starting/ending of cultivation or occurrences of snow cover. Surface wind and temperature gradient data around the forests confirmed that nocturnal downslope winds contributing to the development of the cold-air pool were especially enhanced in the dormant season in cases of highland-scale strong radiative cooling days. In a previous studies, Chen and Yi (2012) noted that optimal conditions for katabatic flows within the canopies are controlled not only by the slope angle but also by the canopy structure. Additionally, Kiefer and Zhong (2013) demonstrated that the nocturnal temperature inversion in a valley was controlled by the amount of sidewall vegetation. Therefore, we concluded that LAI changes in the mountain forest affected seasonal changes in the development of a nocturnal cold-air pool in the Sugadaira Highland. This also means that temperature records at the Sugadaira AMeDAS, one of the representative JMA stations with a high elevation in Nagano Prefecture, are also affected by forest phenology.

According to the heat budget analysis, the heat-amount difference in cold-air pool development before and after the LAI changes was nearly the same or smaller than the total storage heat flux of forest in the previous studies. Temporal fluctuations of the nocturnal temperature differences between the AME and SRS1, indicating the NTI in the basin, corresponded to the observed *Rn* fluctuation at the CGS due to cloud amount changes in several 10 W/m^2 (figures omitted). Therefore, the order of estimated heat flux difference (*Ldif*), such as in several W/m^2, is also reasonable to impact on cold-air pool development. The results indicated that daytime forest heat-storage variabilities can compensate for nocturnal radiative cooling from the canopy. On the other hand, the effects of LAI changes on the dynamics of catchment-scale drainage flow are rather complicated. For instance, Yi et al. (2005) revealed the presence of a very stable layer at the maximum leaf area density in a subalpine forest and that nighttime drainage flows in the forest are restricted to a relatively shallow layer of air beneath the canopy. Yi (2008) also demonstrated that Reynolds stress to characterize the S-shaped wind profile (Shaw 1977) of drainage flows in the forest can be predicted by the LAI. Namely, the difference in LAI changes— not only the balance between radiative cooling and heat flux at canopy level but also the wind speed and stability profile in the forest—could modify the heat advection with downslope winds from the forests. Such dynamics would modify the development speed of the cold-air lake and its depth, which this study could not evaluate. At the same time, forest distribution is not uniform but patchy in the Sugadaira Highland (Fig. 6a), and katabatic flows on the upper grasslands may be hampered by the calm air mass in the downstream forests during the growing season. To understand the mechanism of three-dimensional discharges from the forested areas according to the LAI changes, we need to deploy a dense microclimate observation network with modeling strategy. Especially, numerical simulation which could present a realistic forest structure/distribution is expected, along with the preparation of observed boundary-condition data.

The timing of observed leaf expansion/fall varied over several weeks depending on the year, for instance, earlier snow melts for several weeks in 2020 did not accompany earlier leaf expansion. Furthermore, the areal estimated LAI showed later greening and earlier leaf fall at the basin bottom than at the SRS elevation. Schuster et al. (2014) also pointed out that cold-air pools have a considerable impact on the growth period of deciduous trees. This evidence raises interesting questions, such as whether upper-stream LAI changes could control the downstream LAI through the weakening of NTI during a dormant season as feedback if the ECT is a key factor. Then which ECT sub-season is important for leaf expansion? Detailed identification of the spatial LAI changes using fine constellation satellite data, such as by the Sentinel mission by the European Space Agency, is expected.

The Sugadaira basin is only part of the upstream hollow in complex terrains, and the cold-air drainage flows finally accumulate in the downwind areas such as the Ueda basin, where human activities are concentrated. Further studies are anticipated to assess the impact of forest phenology in the mountain range on the nocturnal climate inland.

Data Availability Statement

The LAI datasets generated in this study are available from the corresponding author on reasonable request.

Acknowledgments

This study was supported by a field research project of the Mountain Science Center in 2018–2019. The aerial photograph in Fig.1c was provided by the SRS. Meteorological observation sites were provided by Sugadaira Farm, Sania Park Sugadaira, and Versoix. Mr. R. Kanai (SRS) continuously supported the forest-tower observation, and Mr. S. Shimizu provided the statistical information about cropland occupation rate. Mr. H. Komaki (University of Tsukuba) provided advice on the identification of tree species. The authors are deeply grateful to all of them for supporting this study.

References

Arx, G., E.G. Pannatier, A. Thimonier, and M. Rebetez, 2013: Microclimate in forests with varying leaf area index and soil moisture: potential implications for seedling establishment in a changing climate. *Journal of Ecology,* **101**:1201-1213. https://doi.org/10.1111/1365-2745.12121

Bernhofer, C., M. Aubinet, R. Clement, A. Grelle, T. Grunwald, A. Ibrom, P. Jarvis, C. Rebmann, E.D. Schulze, and J.D. Tenhunen, 2003: Spruce forests (Norway and Sitka spruce, including Douglas fir): carbon and water fluxes, balances, ecological and ecophysiological determinants. In: Valentini, R. (ed.) Fluxes of carbon, water and energy of European forests. *Ecological Studies*, **163**, 99–123.

Bosman, P.J.M, C.C. van Heerwaarden, and A.J. Teulin, 2018: Sensible heating as a potential mechanism for enhanced cloud formation over temperate forest. *Quarter. J. Royal Meterol. Soc*., **145**, 450–468.

Chen, H., and C. Yi, 2012: Optimal control of katabatic flows within canopies. *Q. J. R. Meteorol.*, **138**, 1676–1680.

Defourny, P., S. Bontemps, C. Lamarche, C. Brockman, M. Herold, G. Kirches, C. Lamarche, V. Kalogirou, F.M. Seifert, and O. Arino, 2017: Land cover CCI: product user guide version 2.0. European Space Agency.

De Frenne, P., F. Rodríguez-Sánchez, D.A. Coomes, L. Baeten, G. Verstraeten, M. Vellend, M. Bernhardt-Römermann, C.D. Brown, J. Brunet, J. Cornelis, G.M. Decocq, H. Dierschke, O. Eriksson, F.S. Gilliam, R. Hedl, T. Heinken, M. Hermy, P. Hommel, M.A. Jenkins, D.L. Kelly, K.J. Kirby, F.J.G. Mitchell, T. Naaf, M. Newman, G. Peterken, P. Petřík, J. Schultz, G. Sonnier, H.V. Calster, D.M. Waller, G. Walther, P.S. White, K.D. Woods, M. Wulf, B.J. Graae, and K. Verheyen, 2013: Microclimate moderates plant responses to macroclimate warming. *Proc Natl Acad Sci,* **110**(46), 18561–18565. https://doi.org/10.1073/pnas.1311190110

Devito, A.S., and D.R. Miller, 1983: Some effects of corn and oak forest canopies on cold air drainage. *Agric. For. Meteorol,* **29,** 39–55. https://doi.org/10.1016/0002-1571(83)90074-2

Diaz, H.F., M. Grosjean, and L. Graumlich, 2003: Climate variability and change in high elevation regions: past, present and future. *Clim. Change,* **59,** 1-4. https://doi.org/10.1023/A:1024416227887

Dorninger, M., C.D. Whiteman, B. Bica, S. Eisenbach, B. Pospichal, and R. Steinacker, 2011: Meteorological events affecting cold-air pools in a small basin. *J. Appli. Met. Clim.*, **50**, 2223–2234. https://doi.org/10.1175/2011JAMC2681.1

Ellison, D., C.E. Morris, B. Locatelli, D. Sheil, J. Cohen, D. Murdiyarso, V. Gutierrez, M. Noordwijk, I.F. Creed, J. Pokorny, D. Gaveau, D.V. Spracklen, A.B. Tobella, U. Ilstedt, A.J. Teuling, S.G. Gebrehiwot, D.C. Sands, B. Muys, B. Verbist, E. Springgay, Y. Sugandi, and C.A. Sullivan, 2017: Trees, forests and water: cool insights for a hot world. *Global Environmental Change,* **43**, 51-61. https://doi.org/10.1016/j.gloenvcha.2017.01.002

Froelich, N.J., C.S.B. Grimmond, and H.P. Schmid, 2011: Nocturnal cooling below a forest canopy: model and evaluation. *Agric. For. Meteorol.*, **151**, 957–968. https://doi.org/10.1016/j.agrformet.2011.02.015

Garratt, J.R., 1992: The atmospheric boundary layer. Cambridge University Press, Cambridge, p. 316.

Geiger, R., R.H. Aron, and P. Todhunter, 2003: The climate near the ground, 6th ed. Rowman and Littlefield, Lanham, 600 pp.

Hall, D.K., and G.A. Riggs, 2016: MODIS/Terra Snow Cover Daily L3 Global 500m SIN Grid, Version 6. Boulder, Colorado USA. NASA National Snow and Ice Data Center Distributed Active Archive Center. https://doi.org/10.5067/MODIS/MOD10A1.006

Hardwick, S.R., R. Toumi, M. Pfeifer, E.C. Turner, R. Nilus, and R.M. Ewers, 2015: The relationship between leaf area index and microclimate in tropical forest and oil palm plantation: forest disturbance drives changes in microclimate. *Agric. For. Meteorol.*, **201**, 187–195. https://doi.org/10.1016/j.agrformet.2014.11.010

Hersbach, H., B. Bell, P. Berrisford, S. Hirahara, A. Horányi, J. Muñoz-Sabater, J. Nicolas, C. Peubey, R. Radu, D. Schepers, A. Simmons, C. Soci, S. Abdalla, X. Abellan, G. Balsamo, P. Bechtold, G. Biavati, J. Bidlot, M. Bonavita, G. De Chiara, P. Dahlgren, D. Dee, M. Diamantakis, R. Dragani, J. Flemming, R. Forbes, M. Fuentes, A. Geer, L. Haimberger, S. Healy, R.J. Hogan, E. Hólm, M. Janisková, S. Keeley, P. Laloyaux, P. Lopez, C. Lupu, G. Radnot, P. de Rosnay, I. Rozum, F. Vamborg, S. Villaume, and J. Thépaut, 2020: The ERA5 global reanalysis. *Quarter. J. Royal Meterol. Soc*., **146**, 1999–2049. https://doi.org/10.1175/1520-0442(2000)013<4229:PFODFP>2.0.CO;2

Hogg, E.H., D.T. Price, and T.A. Black, 2000: Postulated feedbacks of deciduous forest phenology on seasonal climate patterns in the western Canadian interior. *J. Climate,* **13**, 4229-4243.https://doi.org/10.1175/1520-0442(2000)013<4229:PFODFP>2.0.CO;2

Iijima, Y., and M. Shinoda, 2000: Seasonal changes in the cold-air pool formation in a subalpine hollow, central Japan. *Int. J. Climatol.*, **20**, 1471–1483.

Iijima, Y., and M. Shinoda, 2002: The influence of seasonally varying atmospheric characteristics on the intensity of nocturnal cooling in a high mountain hollow. *J. Appl. Meteor. Climatol.,* **41**, 734–743.

Kiefer, M.T., and S. Zhong, 2013: The effect of sidewall forest canopies on the formation of cold-air pools: a numerical study. *J. Geophy. Res. Atmosphere*, **118,** 5965–5978. https://doi:10.1002/jgrd.50509.

Kimura, F., and T. Kuwagata, 1993: Thermally induced wind passing from plain to basin over a mountain range. *J. Appl. Meteor*., **32**, 1538–1547. https://doi.org/10.1175/1520-0450(1993)032<1538:TIWPFP>2.0.CO;2

Kondo, J., T. Kuwagata, and S. Haginoya, 1989: Heat budget analysis of nocturnal cooling and daytime heating in a basin. *J. Atmos. Sci.*, **46**, 2917–2933. https://doi.org/10.1175/1520-0469(1989)046<2917:HBAONC>2.0.CO;2

Kudoh, T., H. Tanaka, H. Toritani, and S. Hwang, 1982: Formation of cold air lake in Sugadaira basin. *Geogr. Rev. Jpn.*, **55**, 849–856. https://doi.org/10.4157/grj.55.849 (in Japanese with English summary)

Kume, A., K.N. Nasahara, S. Nagai, and H. Muraoka, 2011: The ratio of transmitted near-infrared radiation to photosynthetically active radiation（PAR）increases in proportion to the absorbed PAR in the canopy. *J. Plant. Res*., **124**, 99–106. https://doi.org/10.1007/s10265-010-0346-1

Kuribayashi, M., H. Oguma, A. Inami, K. Tanaka, and R. Kanai, 2020: Proceeding of autumn meeting of Meteorological Society of Japan, p. 109.

Lee, S.H., and F. Kimura, 2001: Comparative studies in the local circulations induced by land-use and by topography. *Boundary-Layer Meteor.*, **101**, 157–182. https://doi.org/10.1023/A:1019219412907

Mahrt, L., and R. Heald, 2014: Common marginal cold pools. *J. Appl. Met. Clim*., **54**, 339–351. https://doi.org/10.1175/JAMC-D-14-0204.1

Maki, M., and T. Harimaya, 1988: The effect of advection and accumulation of downslope cold air on nocturnal cooling in basins. *J. Met. Soc. Jap.*, **66**, 581–597.

Maki, M., T. Harimaya, and K. Kikuchi, 1986: Heat budget studies on nocturnal cooling in a basin. *J. Met. Soc. Jap.*, **64**, 727–741.

Mencuccini, M., J. Grace, J. Moncrieff, and K.G. McNaughton, 2003: Forests at the land-atmosphere interface. CABI Publishing Press, UK, 304 pp.

Menzel, A., T.H. Sparks, N. Estrella, E. Koch, A. Aasa, R. Ahas, K. Alm-Kubler, P. Bissolli, O. Braslavska, A. Briede, F.M. Chmielewski, Z. Crepinsek, Y. Curnel, A. Dahl, C. Defila, A. Donnelly, Y. Filella, K. Jatcza, F. Mage, A. Mestre, O. Nordli, J. Penuelas, P. Pirinen, V. Remisova, H. Scheifinger, M. Striz, S. Susnik, A.J.H. Van Vliet, F.E. Wielgolaski, S. Zach, and A. Zust, 2006: European phenological response to climate change matches the warming pattern. *Glob. Change Biol.*, **12**, 1969–1976. https://doi.org/10.1111/j.1365-2486.2006.01193.x

Moderow, U., M. Aubinet, C. Feigenwinter, O. Kolle, A. Lindroth, M. Mölder, L. Montaganai, C. Rebman, and C. Bernhofer, 2009: Available energy and energy balance closure at four coniferous forest sites across Europe. *Theor. Appl. Climatol.*, **98**, 397–412. https://doi.org/10.1007/s00704-009-0175-0

Motohka T., K.N. Nasahara, H. Oguma, and S. Tsuchida, 2010: Applicability of green–red vegetation index for remote sensing of vegetation phenology. *Remote Sens.*, **2**, 2369–2387.

Nagai, S., T.M. Saitoh, K.N. Nasahara, and R. Suzuki, 2015: Spatio-temporal distribution of the timing of start and end of growing season along vertical and horizontal gradients in Japan. *Int. J. Biometeorol*., **59**, 47–54. https://doi.org/10.1007/s00484-014-0822-8

Nakamura, K., 1976: Nocturnal cold air drainage and distribution of air temperature on the gentle slope. *Geogr. Rev. Jpn*., **49**, 380–387. https://doi.org/10.4157/grj.49.380 (in Japanese with English summary)

Nakamura, K., 1978: Appearance and drainage areas of the cold air stream on the slope of Mt. Omatsu, Sugadaira, Central Japan. *Geogr. Rev. Jpn.*, **51**, 793–803. https://doi.org/10.4157/grj.51.793 (in Japanese with English summary)

Nasahara, K.N., H. Muraoka, S. Nagai, and H. Mikami, 2008: Vertical integration of leaf area index in a Japanese deciduous broad-leaved forest. *Agric. For. Meteorol.*, **148**, 1136–1146. https://doi.org/10.1016/j.agrformet.2008.02.011

Oliphant, A.J., C.S.B. Grimmond, H.N. Zutter, H.P. Schmid, H.B. Su, S.L. Scott, B. Offerle, J.C. Randolph, and J. Ehman, 2004: Heat storage and energy balance fluxes for a temperate deciduous forest. *Agric. For. Meteorol.*, **126,** 185–201. https://doi.org/10.1016/j.agrformet.2004.07.003

Pellerin, M., A. Delestrade, G. Mathieu, O. Rigault, and N.G. Yoccoz, 2021: Spring tree phenology in the Alps: effects of air temperature, altitude and local topography. *European Journal of Forest Research*, **131**, 1957-1965.

Petkovsek, Z., 1992: Turbulent dissipation of cold air lake in a basin. *Meteor. Atmos. Phys.*, **47**, 237–245. https://doi.org/10.1007/BF01025620

Saitoh, T.M., I. Tamagawa, H. Muraoka, and H. Koizumi, 2010: Heat storage due to photosynthesis and respiration activities in forests. *J. Agric. Meteorol*., **66**, 289–298. https://doi.org/10.2480/agrmet.66.4.9 (in Japanese with English summary)

Schuster, C., M. Kirchner, G. Jakobi, and A. Menzel, 2014: Frequency of inversions affects senescence phenology of *Acer pseudoplatanus* and *Fagus sylvatica*. *Int. J. Biometeorol.*, **58**, 485–498. https://doi.org/10.1007/s00484-013-0709-0

Shaw, R. H., 1977: Secondary wind speed maxima inside plant canopies, *J. Appl. Meteorol*., **16**, 514–521.

Staebler, R.M., and D.R. Fitzjarrald, 2005: Measuring canopy structure and the kinematics of subcanopy flows in two forests. *J. Appl. Meteorol*., **44**, 1161–1179. https://doi.org/10.1175/JAM2265.1

Swenson, S., S.P. Burns, and D.M. Lawrence, 2019: The impact of biomass heat storage on the canopy energy balance and atmospheric stability in the community land model, *J. Adv. Modeling Earth Syst*., **11**, 83–98.

Tachibana, Y., 1995: A statistical study of the snowfall distribution on the Japan Sea side of Hokkaido and its relation to synoptic-scale and meso-scale environments. *J. Met. Soc. Jap.,* **73**, 697–715. https://doi.org/10.2151/jmsj1965.73.3_697

Tadaki, Y., H. Kitamura, K. Kanie, H. Sano, A. Shigematsu, and S. Ohtsu, 1994: Leaf opening and falling of Japanese larch at different altitudes. *Jpn. J. Ecol.*, **44**, 305–314. https://doi.org/10.18960/seitai.44.3_305 (in Japanese with English summary)

Toritani, H., 1985: Formation of cold air lake and cold air drainage in the Sugadaira basin, Nagano Prefecture, Japan. *Geogr. Rev. Jpn*., **58,** 67–79. https://doi.org/10.4157/grj1984a.58.2_67 (in Japanese with English summary)

Uehara, G., M. Nishimura, A. Sasaki, and K. Suzuki, 2020: The influence of snow cover for the local wind system on the east slope of Mt. Norikura. *Tenki*, **67**, 395–406. https://doi.org/10.24761/tenki.67.7_395 (in Japanese with English summary)

Ueno, K., J. Isono, F. Imaizumi, A. Inami, R. Nakai, K. Suzuki, H. Kobayashi, I. Tamagawa, T.M. Saitoh, and H. Kondo, 2013: Data archive of meteorological data created through the Japanese Alps Inter-University Cooperative Project. *Journal of Geography (Chigaku Zasshi)*, **122**, 638–650 https://doi.org/10.5026/jgeography.122.638 (in Japanese with English abstract)

Ueno, K., K. Kurobe, F. Imaizumi, and R. Nishii, 2015: Effects of deforestation and weather on diurnal frost heave processes on the steep mountain slopes in south central Japan. *Earth Surf. Process Landf*., **40**, 2013–2025. https://doi.org/10.1002/esp.3776

Ueno, K., S. Ueda, R. Kanai, D. Masaki, M. Sato, S. Rin, and M. Hirota, 2017: Diurnal and seasonal variation of air temperature profile in the mountain forest at Sugadaira, central Japan. *Tsukuba Geoenviron. Sci.*, **13**, 1–12. https://doi.org/10.15068/00150208

Ueno, K., Y. Watarai, A. Kusada, N. Hirose, and S. Shimizu, 2007: Spatial heterogeneity of snow covers in Sugadaira, central Japan. *Tsukuba Geoenviron. Sci*., **3**, 33–39.

Vitasse, Y., A.J. Porte, A. Kremer, R. Michalet, and S. Delzon, 2009: Responses of canopy duration to temperature changes in four temperate tree species: relative contributions of spring and autumn leaf phenology. *Oecologia*, **161**, 187–198. https://doi.org/10.1007/s00442-009-1363-4

Wang, X., C. Wang, and Q. Li, 2015: Wind regimes above and below a temperate deciduous forest canopy in complex terrain: interactions between slope and valley winds. *Atmosphere*, **6**, 60–87. https://doi.org/10.3390/atmos6010060

Wilson, K.B., and D.D. Baldocchi, 2000: Seasonal and interannual variability of energy fluxes over a broadleaved temperate deciduous forest in North America. *Agric. For. Meteorol.,* **100**, 1–18.

Wilson, K.B., P. J. Hanson, and D.D. Baldocchi, 2000: Factors controlling evaporation and energy partitioning beneath a deciduous forest over an annual cycle. *Agric. For. Meteorol.,* **102**, 83-103.

Yi, C., 2007: Momentum transfer within canopies. *J. Appl. Met. Clim.* **47**, 262–275.

Yi, C., R.K. Monson, Z. Zhai, D. E. Anderson, B. Lamb, G. Allwine, A. A. Turnipseed, and S. P. Burns, 2005: Modeling and measuring the nocturnal drainage flow in a high-elevation, subalpine forest with complex terrain. *J. Geophysical Res*., **110**, D22303.

Figures

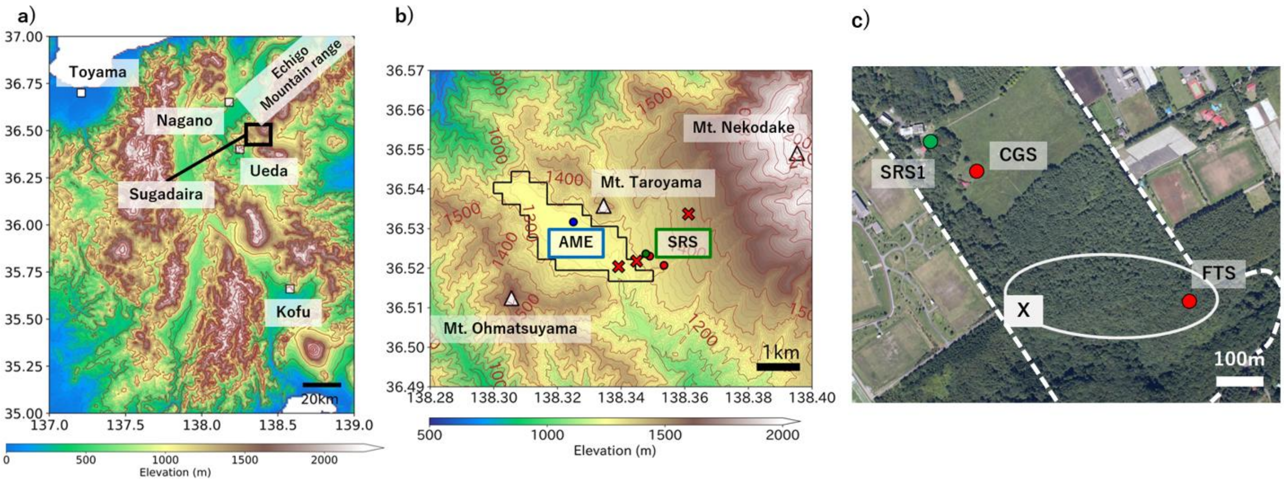

Fig. 1 (a) Topography of central Japan, showing the location of the Sugadaira Highland (black box), (b) topography around the Sugadaira basin (surrounded by a solid line), with observation points of the AME (blue mark), SRS (green mark), and temporal temperature observations (red crosses); and (c) land cover at the SRS (surrounded by white dashed lines) with the locations of observation sites (SRS1, CGS and FTS) and a location of mixed forest (X). The aerial photograph was taken in 2011 and provided by the SRS.

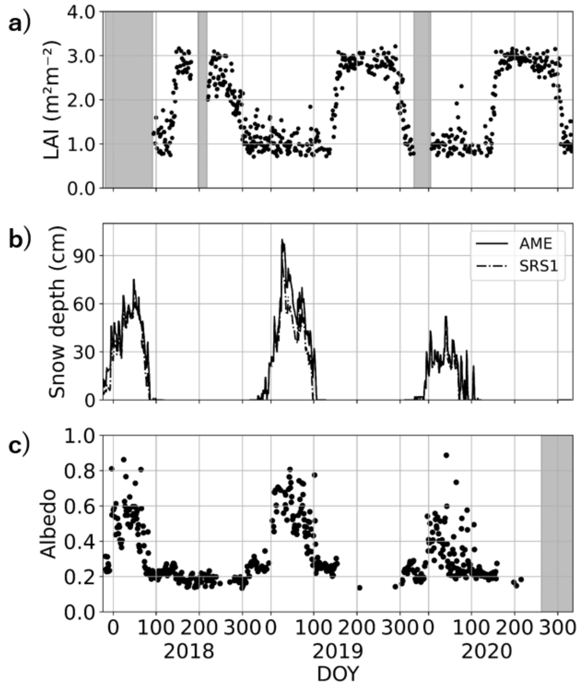

Fig. 2 (a) Seasonal changes in the daily LAI at the FTS, (b) daily maximum snow depth at the AME and SRS1, and (c) daytime average albedo changes at the FTS. Gray areas indicate no data.

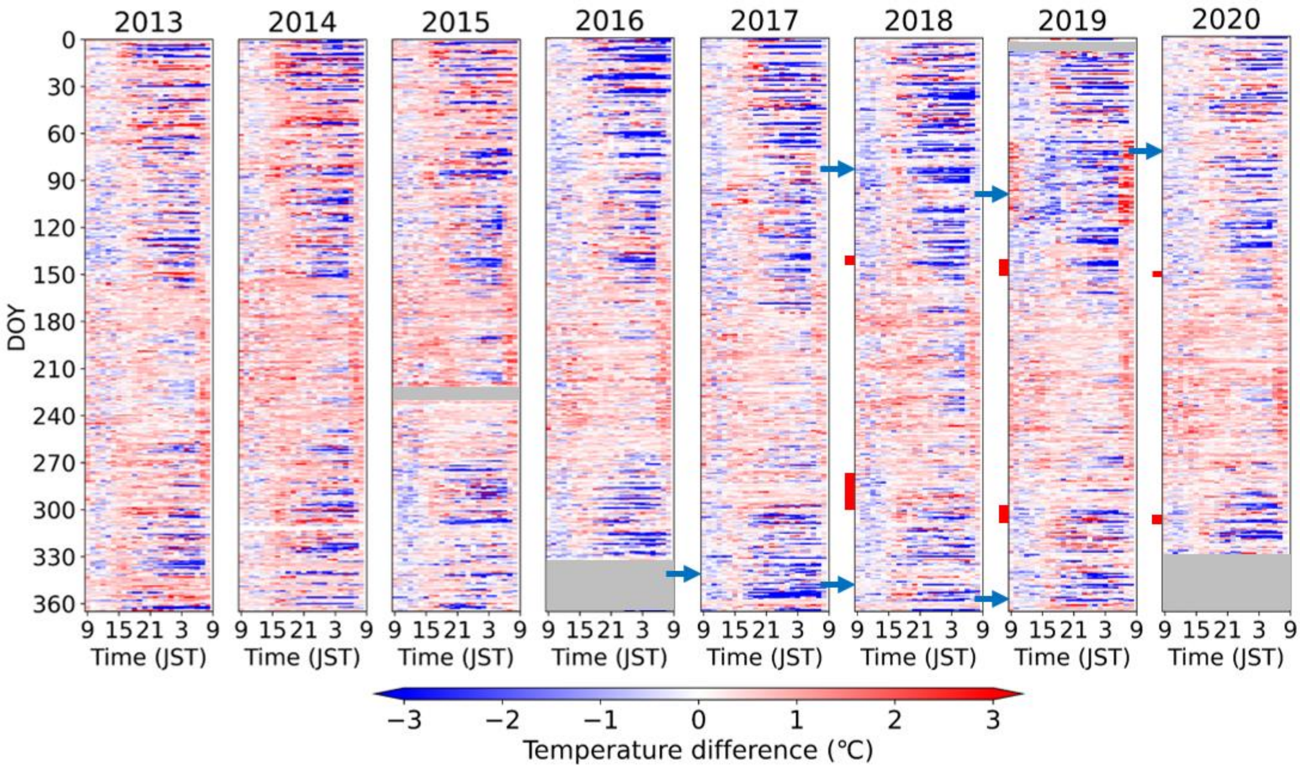

Fig. 3 Time–DOY cross sections of the hourly air temperature differences between the AME and SRS1 for eight years. Each column is composed using the time sequence as a function of DOY and local time starting at 9:00 JST. Blue (red) areas indicate cooler (warmer) temperatures at the AME than at the SRS1. Leaf expansion/fall seasons in Fig. 2a are shown as red vertical bars, and the start and end of snow-cover seasons in Fig. 2b are indicated by blue horizontal arrows. Gray areas indicate no data.

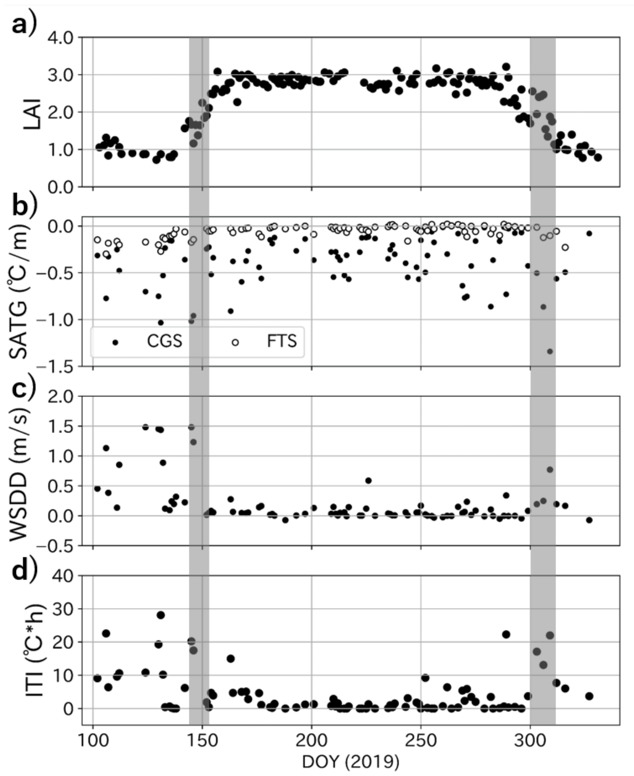

Fig. 4 Time sequences of the (a) daily LAI, (b) nocturnal SATG (normalized by sensor hight) at the CGS and FTS, (c) nocturnal WSDD at the CGS, and (d) ITI in April–December 2019 . Gray bars indicate seasons of leaf expansion/fall at the FTS.

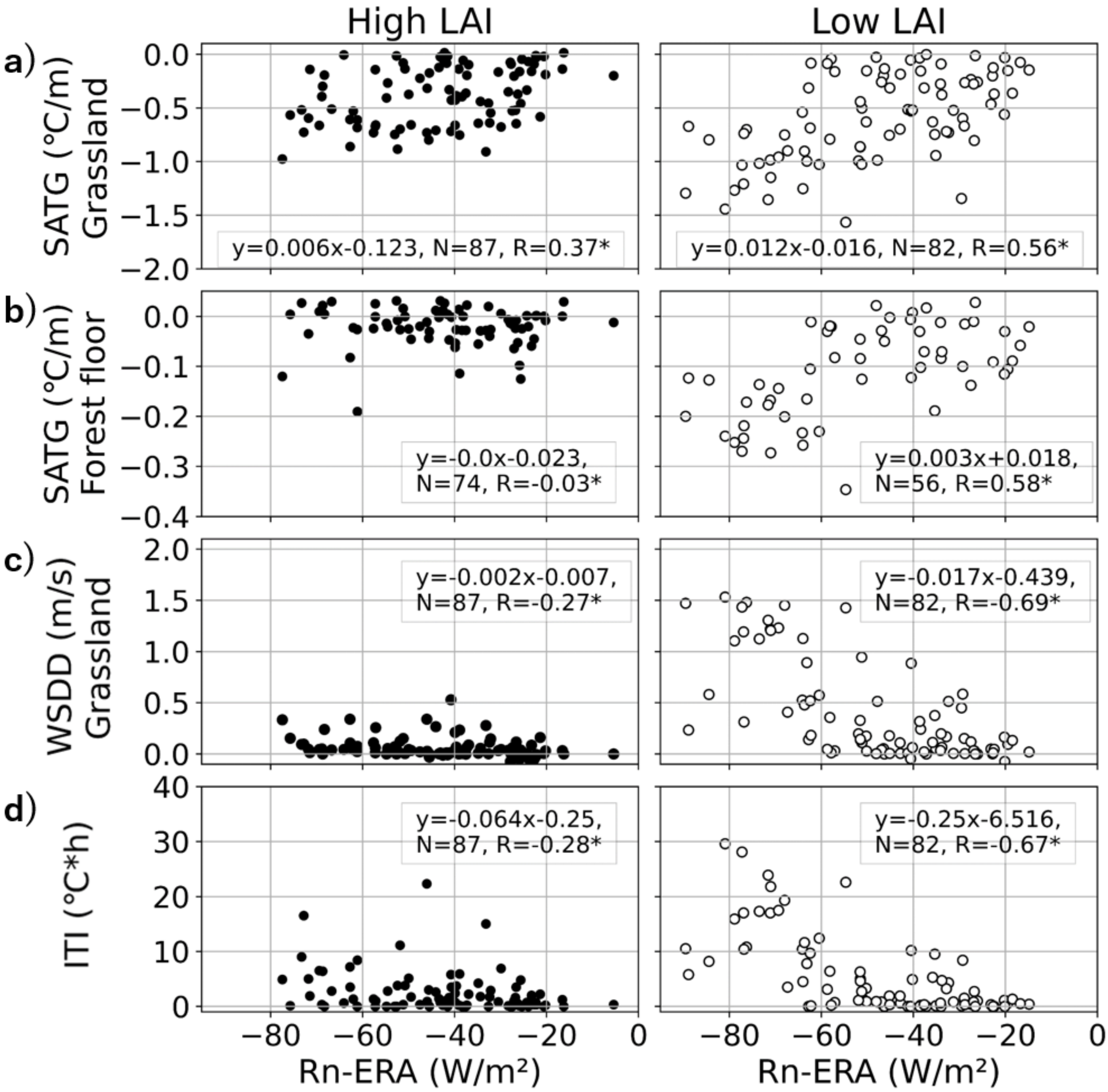

Fig. 5 Nocturnal averaged SATG at the (a) grassland and (b) forest floor as a function of Rn-ERA. The same for WSDD at the grassland (c) and ITI (d). Left (right) figures indicate a daily LAI of more (less) than 2.5 (1.0). R and N correspond to the correlation coefficient and sample number for linear regression, respectively, and * is the significant correlation at the 1% level.

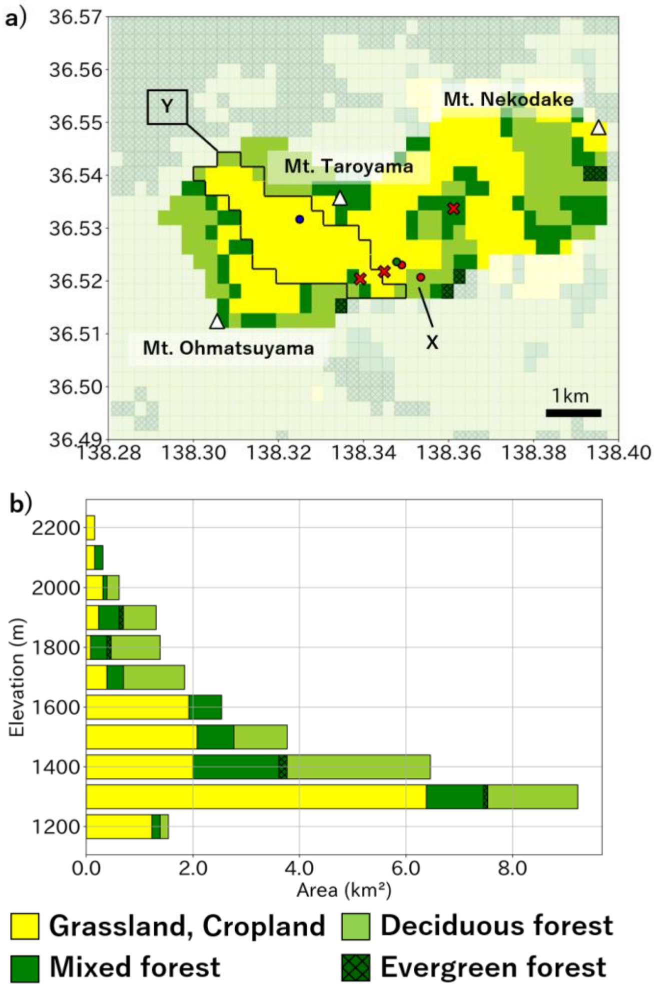

Fig. 6 (a) Estimated drainage areas (highlight yellow and green colors) with land cover and observation points. A solid black area, Y, indicates the basin bottom, and X indicates the location of mixed forest at the SRS. (b) Altitudinal changes in areas depending on the land cover.

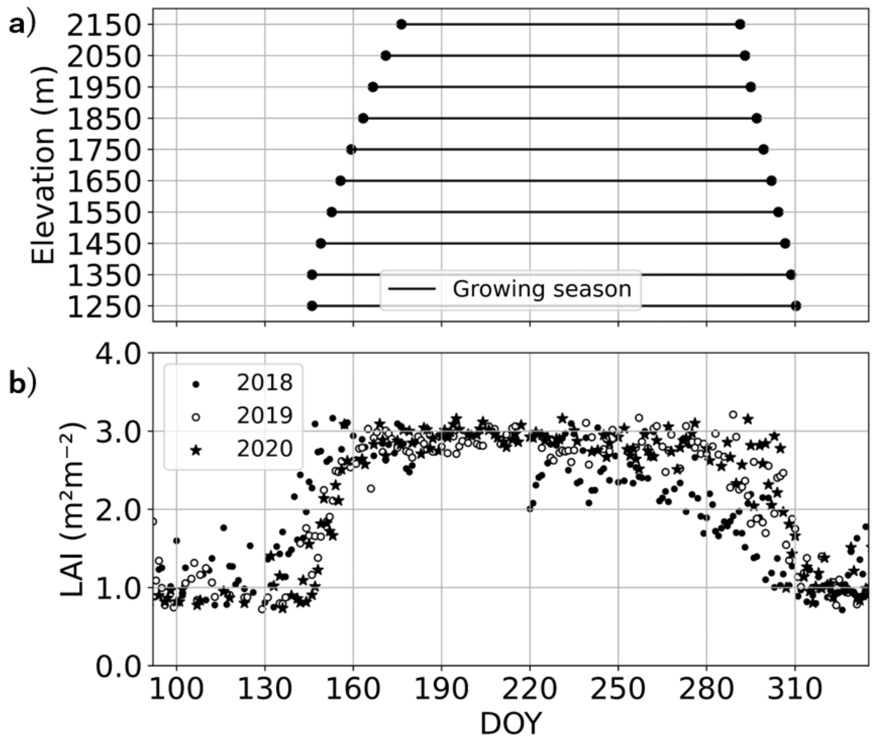

Fig. 7 Seasonal changes in (a) estimated growing seasons (including leaf-expansion and leaf-fall seasons) depending on altitude and (b) the daily LAI at the FTS for three years.

Table. 1 Seasonality of (a) forest phenology measured using the LAI at the FTS and (b) periods of snow cover at the SRS1.

a)

	2018	2019	2020
Dormant season (spring)	1st Jan - 20th May	1st Jan - 22nd May	1st Jan - 28th May
Leaf-expansion season	21st May - 24th May	23rd May - 1st Jun	29th May - 1st Jun
Growing season	25th May - 5th Oct	2nd Jun - 24th Oct	2nd Jun - 31st Oct
Leaf-fall season	6th Oct - 28th Oct	25th Oct - 6th Nov	1st Nov - 7th Nov
Dormant season (autumn)	29th Oct - 31st Dec	7th Nov - 31st Dec	8th Nov - 31st Dec

b)

	2017 - 2018	2018 - 2019	2019 - 2020
Snow free	- 1st Dec	- 1st Dec	- 2nd Dec
Snow cover	5th Dec - 25th Mar	14th Dec - 7th Apr	22nd Dec - 11th Mar
Snow free	26th Mar -	10th Apr -	25th Apr -